Research Article

Synthesis and characterization of novel organic–inorganic hybrid nanocomposites of phosphate–benzimidazole by soft chemistry route in aqueous media

Halima El aadad[1] · **Driss Rair**[1] · **Abdelkrim Chahine**[1]

Received: 4 May 2019 / Accepted: 10 October 2019 / Published online: 24 October 2019

Abstract
In this work, novel organic–inorganic hybrid nanocomposites M^{+}/PO_3^{-} (M = 2,2′-dibenzimidazolyl butane) were prepared by soft chemistry method. The synthesis was done by ion exchange method between sodium metaphosphate anions ($yNaPO_3$) and 2,2′-dibenzimidazolyl butane dichlorhydrates cations ($xMCl_2$) in aqueous media. The MCl_2 organic salt and the M^{+}/PO_3^{-} hybrid nanocomposites were characterized by using spectroscopic and microscopic analyses. The FTIR and Raman spectroscopy are showed new bands in the hybrid nanocomposites structure, which proved the interactions between PO_3 and NH of MCl_2 molecules. The UV–Vis results of MCl_2 and M^{+}/PO_3^{-} materials showed a broad absorption band in 200–300 nm regions, originating from phosphate and benzimidazole molecules. The X-ray diffraction was showed the appearance of new peaks attributed to the phosphate (PO_3) and a reduction of the intensity of the benzimidazole peaks. The TEM images are showed changes in appearance and size of hybrid materials. Moreover, the surface of hybrids became less dark and the size of M^{+}/PO_3^{-} nanocomposites diameter was < 50 nm. The EDX analysis results revealed the presence of carbon, oxygen, and phosphate, confirming the interactions between phosphate and MCl_2 organic salt.

Electronic supplementary material The online version of this article (https://doi.org/10.1007/s42452-019-1482-4) contains supplementary material, which is available to authorized users.

✉ Abdelkrim Chahine, abdelkrimchahine@gmail.com; Halima El aadad, halimaelaadad@gmail.com | [1]Laboratory of Physico-Chemistry of Vitreous and Crystallized Materials (LPCVCM), Faculty of Science, Ibn Tofail University, BP 133, 14000 Kenitra, Morocco.

Graphic abstract

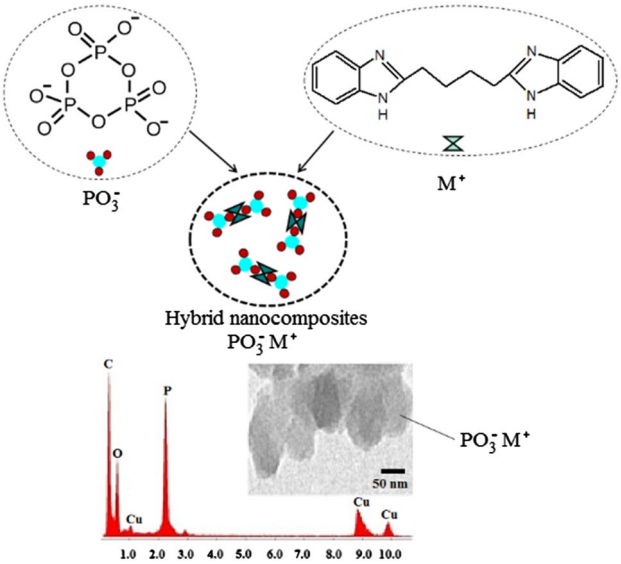

Keywords Hybrid nanocomposites · Soft chemistry · Ion exchange · Benzimidazole · Phosphate

1 Introduction

In the technological world, there are different types of well-established materials like: metals [1], ceramics [2], glasses [3] and plastics [4]. These materials are not enough to satisfy all the needs and technological desires. Furthermore, they should be more inexpensive, recyclable, environmentally friendly with better performance to improve the efficiency of various applications [5–7].

Indeed, the scientists have to design a new field of research, in which their creativity can be fully expressed, to develop new hybrid materials of an inorganic–organic character with a new properties associated with their multifunctionality. In addition, these functionalized materials have innovative industrial applications in extremely varied domains such as: metallic coating [8, 9], anti-corrosion [10], thermal insulation [11], pharmacology [12], pesticides [13], antimicrobial [14], catalysis [15], extraction [16] and membrane separation [17].

The synthesis of hybrid materials by soft chemistry route [18] aroused a strong interest, in both academic and industrial worlds. This method is carried out at low temperature (20–200 °C) in aqueous solutions or organic solvent, from molecular precursors or nanoparticles [19]. Furthermore, it offers the possibility to combine properties of organic and inorganic compounds, to form new hybrid materials, pure, homogeneous with remarkable properties and multifunctionalities for different applications. This process presents advantages over many other methods in control perfectly the stoichiometry, to be inexpensive and to confer high purity on the synthesized material [21].

Phosphate is one of the indispensable minerals for life [20]. However, the development of materials of phosphate has a great interest in different technologies, noticeably in adsorption [21], membrane separation [22], ion exchange [23], biomedical treatment [24] and chemical precipitation [25]. Recently, the hybrid materials of phosphate have received considerable attention [26]. In the broad sense, hybrid phosphate materials combine the different properties of phosphate with those of the organic compound such as: polymers [27] and organic salts [28].

Furthermore, they often have completely new characteristics, according to the space distribution and size of their constituents.

In this work, we have synthesized new organic–inorganic hybrid nanocomposites of phosphate and benzimidazole via a soft chemistry process. The sodium metaphosphate is used as inorganic precursor with different molar ratios ($xMCl_2$–$yNaPO_3$) to study the influence of phosphate content on the structure and properties of hybrid nanocomposites. The structural properties of MCl_2 organic salt and M^+/PO_3^- hybrid nanocomposites are studied by FT-IR, Raman and DRX analysis. The absorption spectra of M^+/PO_3^- hybrids were measured in the UV–visible region. The morphology of surface is characterized by TEM with EDX detector.

2 Materials and methods

2.1 Chemicals and reagents

All reactants and products were used without further purification. The Ortho-phenylenediamine (98%) was purchased from Fluka analytical. The adipic acid (99%) and the hydrochloric acid were obtained from Sigma-Aldrich. The sodium methaphosphate (99%) was purchased from Riedel de Haën. In all cases, the distilled water was used to prepare the solutions.

2.2 Synthesis of benzimidazole derivative: 2,2′-dibenzimidazolyl butane dichlorhydrates

The mixture of *o*-Phenylenediamine (0.025 mol) and adipic acid (0.0125 mol) were dissolved in 20 mL of hydrochloric acid (4 N). The reaction was refluxed under stirring for 36 h. After completion, the resulting precipitate was filtered, washed, dried and then recrystallized with absolute ethanol to get blue crystal. Yield: 83%, FT-IR (KBr pellet, cm^{-1}): 3330 (N–H), 3085 ((=C–H)Ar), 1628 (C=N), 1563 (N–H_2), 1512 (C=C), 1459 (CH_2/Met), 750 ((=C–H) Ar) cm^{-1}. Raman (cm^{-1}): 3080 (N–H), 2740 ($NH_2^+Cl^-$), 1629 (C=N), 1512 (C=C/Ar), 1450 (CH_2/Met), 750 ((=C–H)Ar) cm^{-1}. The ^{1}H NMR (300 MHz, D_2O, ppm): 1.9 (q,4H), 3.1 (t,3H), 7.43–7.56 (m,8H) ppm. The ^{13}C NMR (100 MHz, D_2O, ppm): 25.56, 113.45, 125.98, 130.38, and 153.05 ppm. ESI–MS: $[M+H]^+$, 291 g/mol, $[M\text{-}H]^+$,289 g/mol. The structure of 2,2′-dibenzimidazolyl butane dichlorhydrates (MCl_2) is shown in Fig. 1.

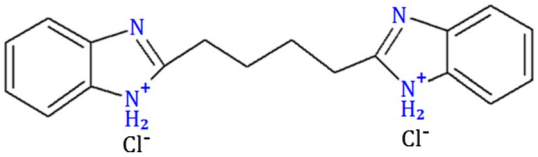

Fig. 1 Molecular structure of 2,2′-dibenzimidazolyl butane dichlorhydrates

2.3 Synthesis of organic–inorganic hybrid nanocomposites of phosphate-benzimidazole

In the present work, the hybrid nanocomposites ($xMCl_2$–$yNaPO_3$) were synthesized by soft chemistry route (Table 1). The synthesis was done by ion exchange process between the sodium metaphosphates anions and the benzimidazole derivative cations (Fig. 2). The synthesis was carried according to the following protocol. To uniformly mix the hybrids species, the precursors were dissolved in an aqueous solution instead of dry mixing.

The benzimidazole powders (0.01 mol) were totally dissolved in 100 mL of distilled water under vigorous magnetic stirring, resulting the formation of a transparent solution. For the mineral solution, the sodium metaphosphate (0.01 mol) was prepared in distilled water (20 mL) under ambient conditions. Afterward, the organic solution is poured properly drop wise into mineral solution, and the hybrids formation was observed.

After completion of reaction in necessitating time, the precipitate was separated by filtration, and dried at 60 °C. The synthesis conditions of hybrid materials are monitored, like: pH, agitation, temperature, and preparation

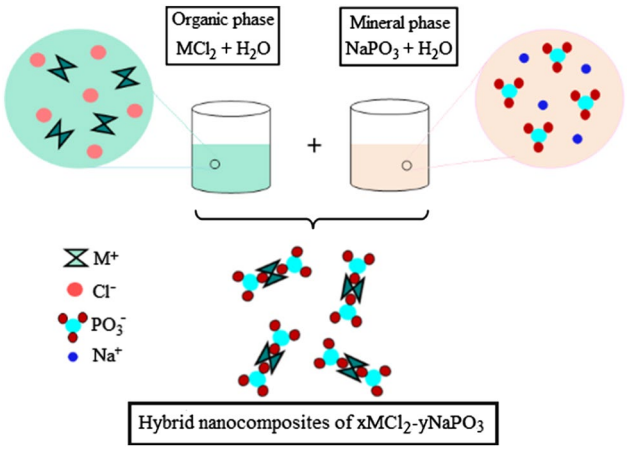

Fig. 2 Schematic representation of synthesis of $xMCl_2$-$yNaPO_3$ hybrid nanocomposites

Table 1 Synthesis of hybrid nanocomposites $xMCl_2$-$yNaPO_3$

Samples	Variables				
	($NaPO_3$)/(MCl_2) molar ratios	$NaPO_3$ (mol)	MCl_2 (mol)	T (°C)	t (min)
MCl_2	–	0	0.01	25	5
MCl_2 + $NaPO_3$ (1)	1:1	0.01	0.01	25	6
MCl_2 + $NaPO_3$ (2)	2:1	0.02	0.01	25	6
MCl_2 + $NaPO_3$ (3)	3:1	0.03	0.01	25	6
MCl_2 + $NaPO_3$ (4)	4:1	0.04	0.01	25	6
MCl_2 + $NaPO_3$ (5)	5:1	0.05	0.01	25	6

time. For the repeatability of results, six tests were performed.

In order to study the morphological and structural properties of hybrid materials, five molar ratios have been synthesized, by changing the phosphate content. The preparation of hybrid materials is carried out by ion exchanges between MCl_2 cations and $NaPO_3$ anions. The molecular structure of benzimidazole derivative MCl_2 has a functional groups NH^+ on which the mineral anions PO_3^- are attached. According to this mechanism, we have the fixation of functional groups M^+ to PO_3^- by forming M^+/PO_3^- hybrid nanocomposites with liberation of the Na^+Cl^- salts.

2.4 Characterization

The Nuclear magnetic resonance (NMR) spectra (ppm) of 2,2′-dibenzimidazolyl butane were recorded with a Bruker AVANCE 300 MHz. The ^1H and ^{13}C NMR spectra were obtained from a 300 MHz. All NMR spectra were measured in D_2O solutions. The molecular weight of 2,2′-dibenzimidazolyl butane was determined by the mass spectrometric method. The Mass spectra have been recorded on a LCQ Advantage MAX-type ion trap spectrometer using Electrospray Ionisation (ESI) techniques.

The structural and spectroscopic properties of phosphate hybrid nanocomposites were studied by infrared and Raman analysis. The Infrared absorption spectra (4000–400 cm^{-1}) have been performed on a Bruker Tensor 27 spectrometer (Bruker, Germany) in KBr phase. The Raman spectra (4000–0 cm^{-1}) have been recorded on a VERTEX 70 with a resolution of 4 cm^{-1}, Nd Yag laser source (1.064 µm) and a nominal power of 500 mW.

The pH was determined with a Hanna precision pH-meter, model 211 (Romania), which was standardized with Bioblock Scientific. The UV/visible/NIR absorption spectra were recorded in JENWEY SERIE 67-UV. The visible radiation UV spectrometer covers the spectral range from 190 to 1100 nm.

The crystal structure of phosphate hybrid nanocomposites was studied by the X-ray diffraction (XRD) by using a diffractometer X'Pert3 Pro MPD Panalytical, with CuKα radiation.

The surface morphology of phosphate hybrid nanocomposites were observed by a transmission electron microscopy (TEM) coupled to a spectroscopy of X-ray energy dispersion (EDX). The measurements were obtained by Tecnai 12 TEM working at 200 kV.

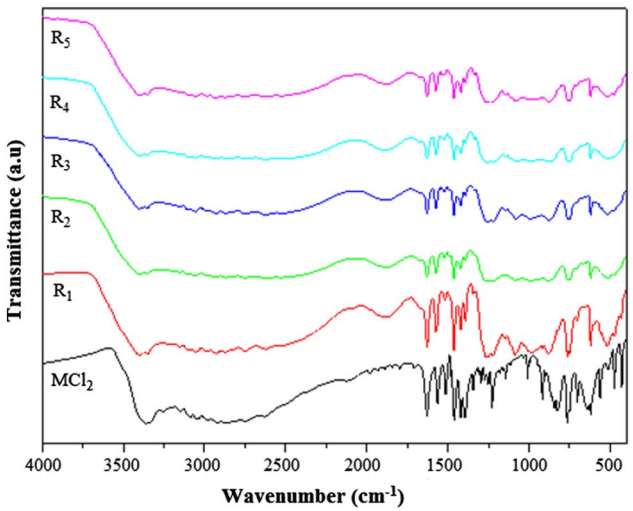

Fig. 3 The FT-IR spectra of MCl_2 organic salt and $xMCl_2$-$yNaPO_3$ hybrid nanocomposites

3 Results and discussion

3.1 FTIR spectroscopy

In order to identify the chemical composition and bonding structure of MCl_2 and M^+/PO_3^- hybrid nanocomposites, the FTIR spectroscopy was used and it was showed in Fig. 3. As seen from Fig. 3, the spectra show several characteristic bands: A strong band at 3330 cm^{-1} is assigned to the stretching vibration of the N–H [29, 30]. The band at 3085 cm^{-1} is attributed to (=C–H)Ar stretching vibration [31]. The band observed at 2917 cm^{-1} is related to the CH_2/Met stretching vibration. The C=N band stretching vibration is appeared at 1628 cm^{-1}. The deformation band of $N–H_2$, which is typical just of pure MCl_2, is assigned to the peak at 1563 cm^{-1}. The peak of the aromatic C=C is showed at 1512 cm^{-1} [32]. A strong absorption band at 750 cm^{-1} is assigned to the stretching deformation of (=C–H) Ar. On the other hand, the spectra of the M^+/PO_3^- hybrid nanocomposites (R_1–R_5) had new bands corresponding to the phosphate groups which are observed in 406–1247 cm^{-1} range. The strong band at 1247 cm^{-1} is assigned to δ_{as}(P–O–P) [33]. The characteristic peak at 1140 cm^{-1} is assigned to the ν_s(O–P–O) [34]. At 986 cm^{-1}, an asymmetric band is observed corresponding to P–O–P stretching vibration [35]. The presence of P–O–P long chains is ascribed to the stretching $\nu_s(PO_2^-)$, appeared at 654 cm^{-1}. The band at 534 cm^{-1} is corresponded to $\delta_{as}(PO_4^{3-})$ groups [36].

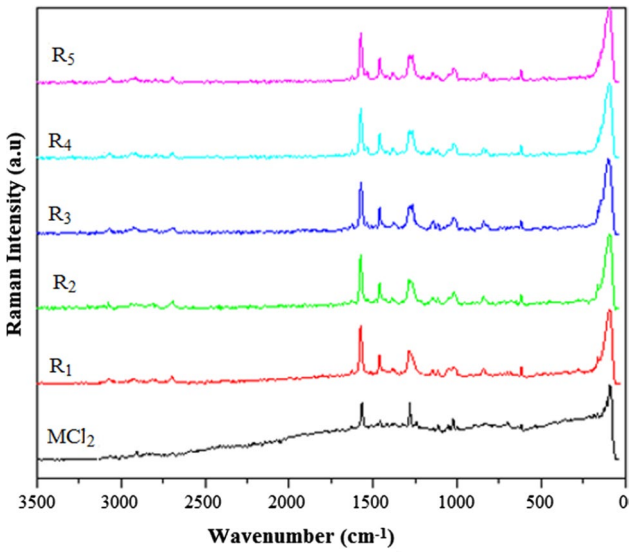

Fig. 4 The Raman spectra of MCl_2 organic salt and $xMCl_2$-$yNaPO_3$ hybrid nanocomposites

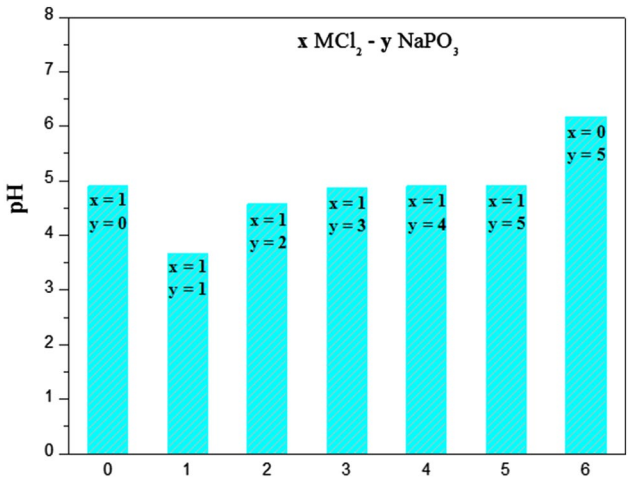

Fig. 5 Monitoring the synthesis of hybrid nanocomposites by pH measurement

3.2 Raman spectroscopy

The Raman measurements were taken to confirm the results of Infrared. The Fig. 4 showed the Raman spectra of MCl_2 and M^+/PO_3^- hybrid nanocomposites. The band at 3067 cm^{-1} is assigned to (=C–H)Ar stretching vibrations [37]. Moreover, the CH_2/Met stretching vibration was appeared at 2906 cm^{-1}. A medium peak observed at 1627 cm^{-1} was provoked by C=N vibration [38]. The stretching vibration of C=C/Ar band is showed at 1567 cm^{-1}. The band observed at 620 cm^{-1} is ascribed to the deformation mode of (=C–H) Ar. Additional bands in the range of 1300–600 cm^{-1} showed the presence of phosphate in the hybrid nanocomposites materials. The bands due to the vibrations of the phosphate group in the M^+/PO_3^- hybrids were observed at 1273 ν_{as}(O–P–O), 1143 ν_s(O–P–O) [39] and 621–843 cm^{-1} ν_{as}(P–O–P) [40]. This result confirms the previous spectra of Infrared which indicate the structural interactions between phosphate and MCl_2 organic product.

3.3 Use of pH measurements to monitor the hybrid nanocomposites synthesis

The synthesis of hybrid nanocomposites was influenced by different parameters such as: concentration, molar ratios, temperature, time reaction and pH [41]. Therefore, these parameters can significantly affect the structure and morphology of hybrid materials [42].

The pH values of the synthesis reaction of hybrid nanocomposites are showed in Fig. 5 Five molar ratios of hybrid nanocomposites ($xMCl_2$)/($yNaPO_3$) (1:1, 1:2: 1:3, 1:4 and 1:5) have been tested respectively. Before the reaction, we are measured separately the pH value of MCl_2 (pH = 4.9) and $NaPO_3$ solutions (pH = 6.1). Therefore, we studied the effect of phosphate content on the M^+/PO_3^- hybrids synthesis and its influence on pH variations. The reaction of the hybrids synthesis is carried out by adding the MCl_2 solution drop wise in the $NaPO_3$ solution.

At 1:1 molar ratio, the initial pH of reaction was 5.7 and the final pH was decreased to 3.6. Therefore, this decrease is explained by the release of protons H^+ by MCl_2 molecules, which weren't reacted because the phosphate content was insufficient. But, the increase of the phosphate concentration in reactions 1:2 (pH = 4.5), 1:3, 1:4 and 1:5 (pH = 4.91) is caused a progressive decrease in the acidity of solutions which is stabilized at 4.91 **(**Fig. 5**).** This decrease is explained by the release of H_2O molecules formed by the OH^- of hydrolysed $NaPO_3$ and the protons of MCl_2 (NH). Furthermore, according to the yields found, the masses of the synthesized hybrids are increased progressively with the phosphate content, which increased the OH^- concentration and decreased the pH values.

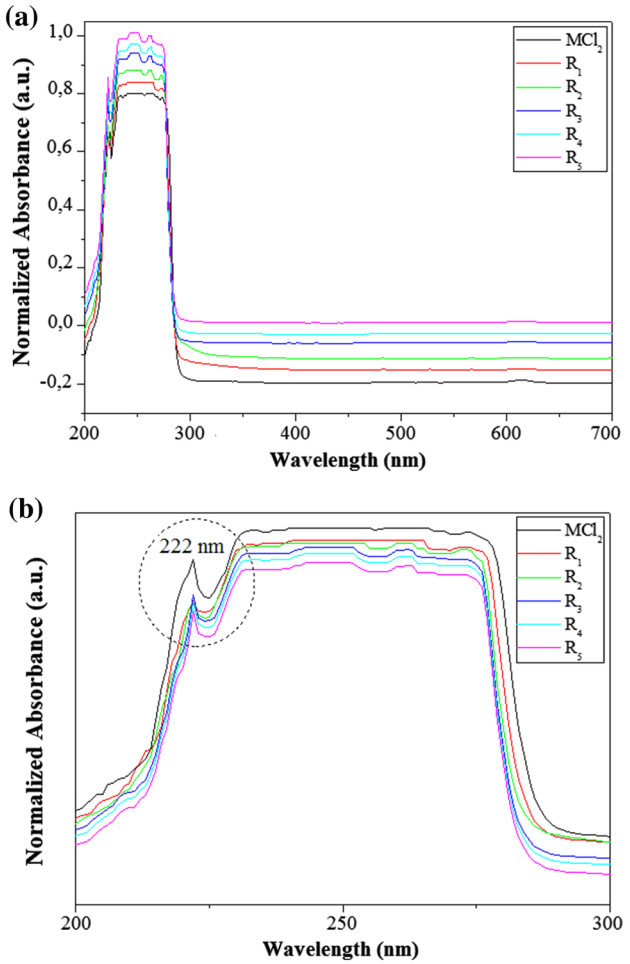

Fig. 6 UV-visible absorption spectra of MCl_2 and $xMCl_2$-$yNaPO_3$ hybrid nanocomposites. **a**: [200–700 nm] and **b**: [200–300 nm]

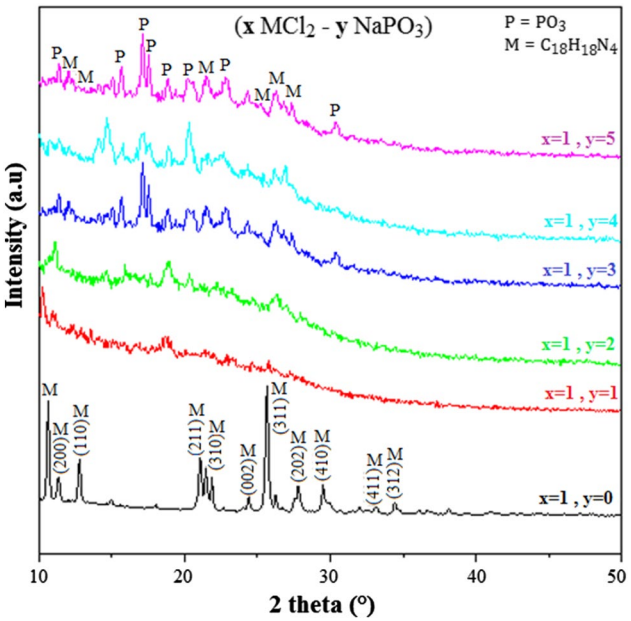

Fig. 7 XRD patterns of MCl_2 organic salt and $xMCl_2$-$yNaPO_3$ hybrid nanocomposites

3.4 UV–visible analysis

The absorption spectra of MCl_2 organic and M^+/PO_3^- hybrid nanocomposites are studied by UV–Vis analysis. The results are registered in the range of 200–700 nm in Fig. 6.

As shown in Fig. 6, all the MCl_2 and M^+/PO_3^- materials showed typical broad peaks at the 200–300 nm region, corresponding to a single transition in the UV region of MCl_2 material. Furthermore, a wide transmission band at around 250 nm corresponds to a similar energy distribution among all the benzimidazole molecules [43]. In addition, according to the results of El Batal et al. [44], the phosphate PO_3^- of hybrid materials revealed an absorption band at around 222 nm (Fig. 6b). As a result, according to the literature data, the MCl_2 and the M^+/PO_3^- materials are characterized by an absorption band which appears in the same region 200–300 nm.

3.5 X-ray diffraction analysis

The X-ray diffraction pattern of MCl_2 and M^+/PO_3^- hybrid nanocomposites with various molar ratios are shown in Fig. 7. The most prominent peaks of MCl_2 particles at 2 theta (°): 11.30 (200), 12.81 (110), 21.02 (211), 21.86 (310), 24.37 (002), 25.63 (311), 27.80 (202), 29.47 (410), 33.17 (411), and 34.35 (312), were well matched with the standard pattern of benzimidazole molecule according to the results found by Vijayan et al. [45]. There is no impurity phase observed, suggesting that the high purity MCl_2 particles were obtained.

The diffraction patterns of M^+/PO_3^- hybrid nanocomposites are showed the appearance of new peaks (P) attributed to strong lines of phosphate (PO_3^-) [46, 47], and an important reduction of the intensity with a widening of benzimidazole peaks (M). The intensity of the peak increased progressively with the phosphate content, which showed the interactions between MCl_2 and $NaPO_3$. These changes can be attributed to a modification in the ordered arrangement of MCl_2 structure, indicating a significant decrease in the crystalline phase and an

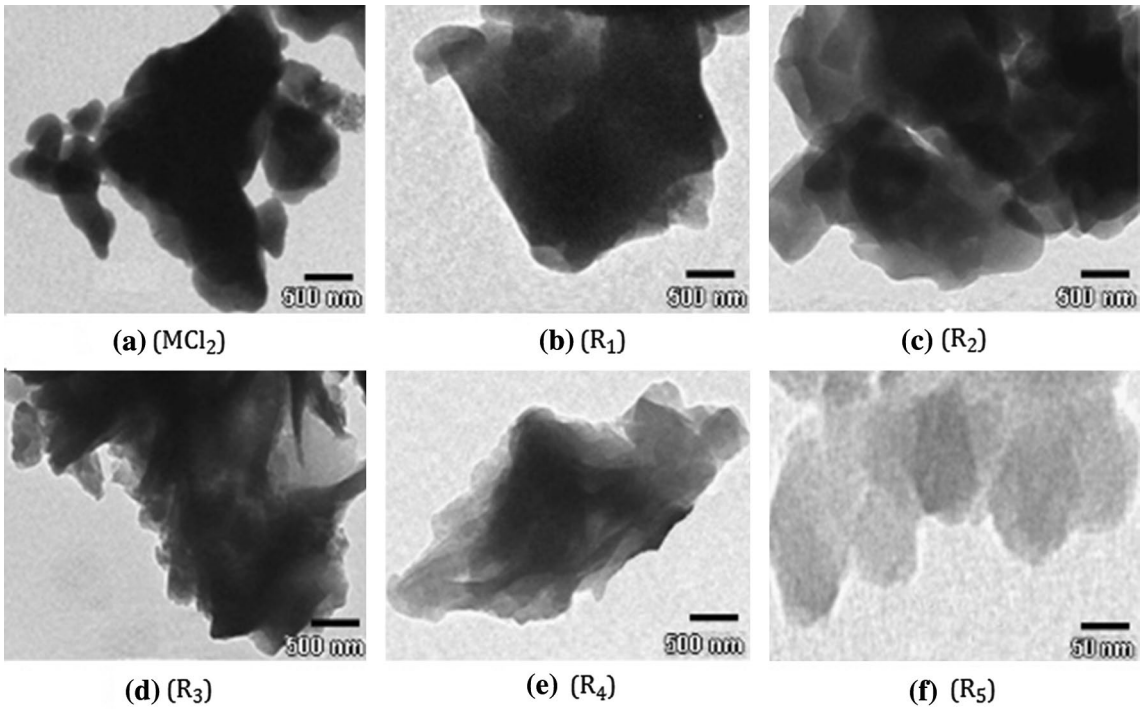

Fig. 8 TEM images of MCl_2 organic salt (**a**) and $xMCl_2$-$yNaPO_3$ hybrid nanocomposites (**b**–**f**)

improvement in the amorphous phases [48, 49]. Therefore, these results confirmed clearly the interactions between MCl_2 and $NaPO_3$ particles.

3.6 The TEM images and elemental analysis using X-EDS

The morphology and size of organic and hybrid nanocomposites are studied by a transmission electron microscopy (TEM) [50]. The TEM images of M^+/PO_3^- hybrid nanocomposites with different molar ratios and their corresponding EDX spectra are presented respectively in the Figs. 8 and 9. The TEM images of Fig. 9 are showed changes in appearance and size with the increase in phosphate content of M^+/PO_3^- hybrid materials (Fig. 8b–f) compared to MCl_2 (Fig. 8a). Indeed, the surface of M^+/PO_3^- hybrid became less dark and the size of hybrid nanocomposites diameter was < 50 nm (Fig. 8e). These TEM observations clearly confirm a morphological transformation of particles from MCl_2 organic salt to M^+/PO_3^- hybrids after 6 min of synthesis.

In addition, the composition of MCl_2 and M^+/PO_3^- hybrid nanoparticles was analyzed using spectroscopy of X-ray energy dispersion (EDX) (Fig. 9). The chemical analysis of MCl_2 is showed the presence of a single element: the carbon that characterizes organic material. On the other hand, after the addition of phosphate, we are noticed the appearance of oxygen and phosphate which characterizes the inorganic material. Therefore, these results are revealed that the phosphate has interacted with the MCl_2 organic salt.

4 Conclusion

The synthesis and characterization of M^+/PO_3^- new hybrid nanocomposites are carried out by soft chemistry method at room temperature. The synthesis was done by ions exchange process between sodium metaphosphates anions and 2,2′-dibenzimidazolyle butane dichlorhydrates cations. The FT-IR and Raman spectra are showed functional groups of the hybrid nanocomposites structure, which combined the both functions of phosphate and MCl_2 and the appearance of new bands which showed the interactions between PO_3 and NH of MCl_2. The UV–Vis absorption spectra of M^+/PO_3^- hybrid nanocomposites have shown a wide transmission band at around 250 nm corresponds to all the Benzimidazole molecules, with the presence of phosphate at 222 nm as the literature reports.

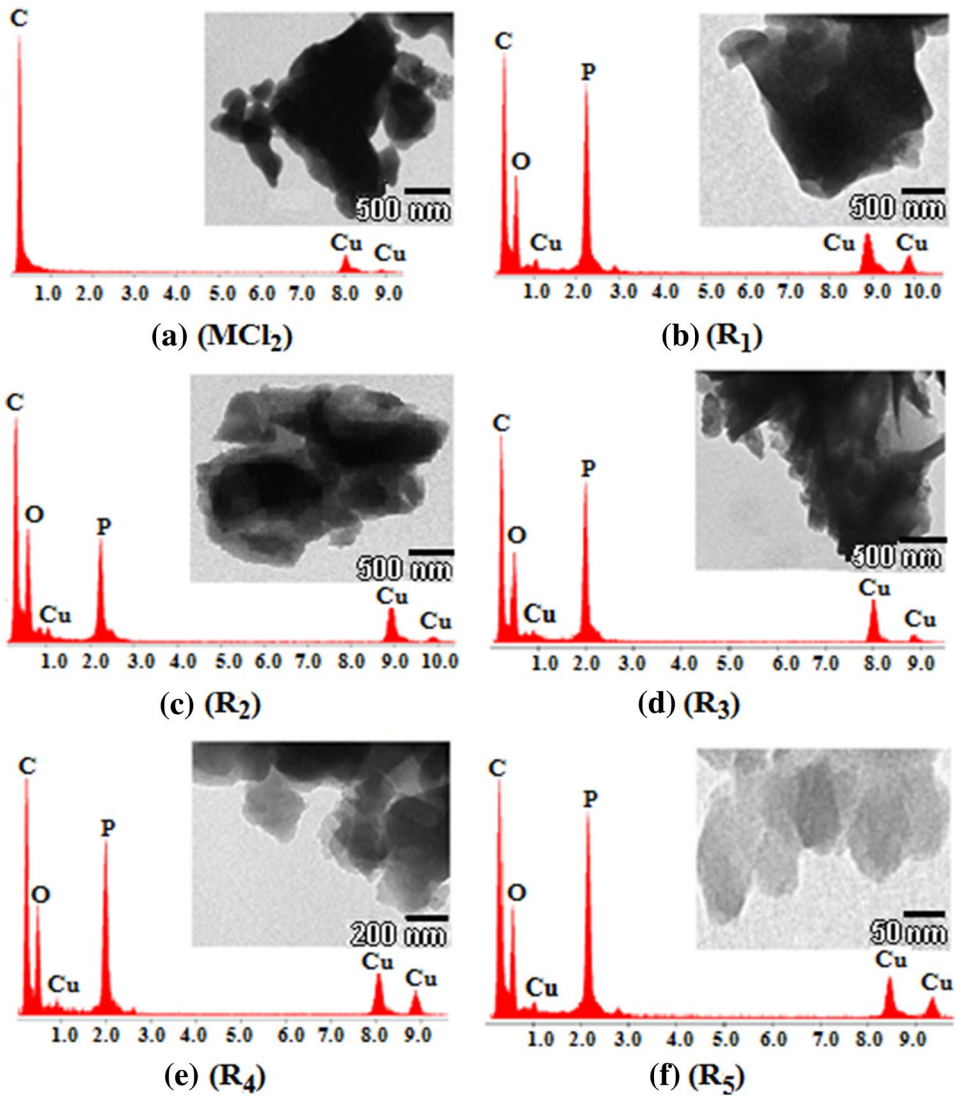

Fig. 9 EDX spectra of MCl_2 organic salt and $xMCl_2$-$yNaPO_3$ hybrid nanocomposites (**b**–**f**)

The X-ray diffraction was showed the appearance of new peaks attributed to the phosphate (PO_3) and a reduction of the intensity of benzimidazole peaks. The observation of the surface morphology by TEM has shown the modification in the surface and the size of M^+/PO_3^- hybrid nanocomposites when the ratio of phosphate increase. These results are confirmed by EDX chemical analysis of hybrid materials, which revealed the presence of carbon, oxygen, and phosphate, confirming the interactions between phosphate and MCl_2 organic salt.

Acknowledgements We are grateful to the Center of Analysis, Expertise, Technology Transfer and Incubation of University Ibn Tofail, for the UV–visible and DRX analysis.

Compliance with ethical standards

Conflict of interest The author(s) declare that they have no competing interests

References

1. Li Guijie et al (2019) Metal complex based delayed fluorescence materials. Org Electron 69:135–152
2. Fu Z et al (2020) Low-fired $Li_2Mg_3ZrO_6$-based composite ceramics with temperature-stable for LTCC applications. J Alloy Compd 812:152001
3. Majjane A et al (2014) X-ray photoelectron spectroscopy (XPS) and FTIR studies of vanadium barium phosphate glasses. Mater Chem Phys 143(2):779–787
4. Dangis A (2018) The usage of recycled plastics materials (rPM) by plastics converters in Europe. Reinf Plast 62(3):159–161
5. Wasalathilake KC et al (2019) Recent advances in graphene based materials as anode materials in sodium-ion batteries. J Energ Chem 42:91–107
6. Jouane Y, Enami Y (2017) Nanolayer-transfer method of TiO_2 slot layers and its application for fabricating hybrid electro-optic polymer/TiO_2 vertical slot waveguide modulators. Opt Laser Technol 94:146–153
7. Wang F et al (2020) Effects of residual carbon materials on the disinfection byproduct formation in artificial and natural waters. Chemosphere 238:124695
8. Kelen MF, de Aguiar Rossi et al (2019) Urethanes PDMS-based: functional hybrid coatings for metallic dental implants. Appl Surf Sci 484:1128–1140
9. Zvonkina IJ, Soucek MD (2016) Inorganic–organic hybrid coatings: common and new approaches. Curr Opin Chem Eng 11:123–127
10. Suzana AF et al (2016) Corrosion protection of chromium-coated steel by hybrid sol-gel coatings. Surf Coat Technol 299:71–80
11. Feng J et al (2016) Silica-cellulose hybrid aerogels for thermal and acoustic insulation applications. Colloids Surf A 506:298–305
12. Haque A et al (2017) Synthesis, characterization, and pharmacological studies of ferrocene-1H-1,2,3-triazole hybrids. J Mol Struct 1146:536–545
13. Nodeh HR et al (2017) Magnetic graphene coated inorganic-organic hybrid nanocomposite for enhanced preconcentration of selected pesticides in tomato and grape. J Chromatogr A 1509:26–34
14. Baartzes N et al (2019) Bioisosteric ferrocenyl aminoquinoline-benzimidazole hybrids: antimicrobial evaluation and mechanistic insights. Eur J Med Chem 180:121–133
15. Jia H et al (2017) Design and fabrication of functional hybrid materials for catalytic applications. Curr Opin Green Sust Chem 4:16–22
16. Radi S et al (2016) Efficient extraction of heavy metals from aqueous solution by novel hybrid material based on silica particles bearing new Schiff base receptor. J Mol Liq 223:112–118
17. Ansaloni L, Deng L (2017) Advances in polymer-inorganic hybrids as membrane materials. Recent Developments in polymer macro, micro and nano blends. Elsevier, Amsterdam, pp 163–206
18. Simo A et al (2018) Shape control VO_2 nanorods prepared by soft chemistry and electrochemical method. Appl Surf Sci 446:145–150
19. Courthéoux Laurence et al (2018) Soft chemistry routes to GeS_2 nanoparticles. Solid State Sci 78:40–45
20. Han C et al (2017) Removal of phosphate using calcium and magnesium-modified iron-based adsorbents. Mater Chem Phys 198:115–124
21. Liu Tao et al (2019) Magnetic zirconium-based metal–organic frameworks for selective phosphate adsorption from water. J Colloid Interface Sci 552:134–141
22. Liu Ruiting et al (2019) Metal–organic framework-based ultrafiltration membrane separation with capacitive-type for enhanced phosphate removal. Chem Eng. J 371:903–913
23. Golubenko DV et al (2018) "An approach to increase the permselectivity and mono-valent ion selectivity of cation-exchange membranes by introduction of amorphous zirconium phosphate nanoparticles. J Membr Sci 563:777–784
24. Salama Ahmed et al (2019) Cellulose/calcium phosphate hybrids: new materials for biomedical and environmental applications. Int J Biol Macromol 127:606–617
25. Li Yongye et al (2019) " Synergistic effect of mesoporous feroxyhyte nanoparticles and Fe(II) on phosphate immobilization: adsorption and chemical precipitation. Powder Technol 345:786–795
26. Matsuura T, Maruyama T (2017) Calcium phosphate-polymer hybrid microparticles having functionalized surfaces prepared by a coaxially electrospray technique. Colloids Surf A 526:64–69
27. Matsuura T et al (2017) Calcium phosphate-polymer hybrid microparticles having functionalized surfaces prepared by a coaxially electrospray technique. Colloid Surf A 526:64–69
28. Saral H et al (2016) Synthesis, spectroscopic characterization and DFT calculations of N-Methyl-2-(2′-hydroxyphenyl) benzimidazole derivatives. J Mol Struct 1103:9–19
29. Ghani NTA, Mansour AM (2011) Palladium(II) and platinum(II) complexes containing benzimidazole ligands: molecular structures, vibrational frequencies and cytotoxicity. J Mol Struct 991(1–3):108–126
30. El aadad H et al (2019) Synthesis, characterization and thermal properties of 2,2′-dibenzimidazolyl butane as a novel corrosion inhibitors for mild steel in sulfuric acid. Surf Rev Lett. https://doi.org/10.1142/S0218625X19501154
31. Mohan S et al (1991) FTIR and Raman studies on benzimidazole. Spectrochim Acta Part A 47(8):1111–1115
32. Kim J-D, Honma I (2005) Anhydrous solid state proton conductor based on benzimidazole/monododecyl phosphate molecular hybrids. Solid State Ion 176(9–10):979–984
33. Férid M et al (1994) Etude du diagramme d'equilibre du systeme $NaPO_3$–Pr $(PO_3)_3$. J Therm Anal 42(5):913–918
34. Bhide A, Hariharan K (2007) Sodium ion transport in $NaPO_3$–Na_2SO_4 glasses. Mater Chem Phys 105(2–3):213–221
35. Rair D et al (2016) Synthesis and study by FTIR, 31P NMR and electrochemical impedance spectroscopy of vanadium zinc phosphate glasses prepared by sol–gel route. J Non-Cryst Solids 432:459–465
36. Vaidhyanathan B et al (1998) Spectroscopic investigations of manganese ions in microwave-prepared $NaPO_3$. PbO glasses. J Phys Chem Solids 59(1):121–128
37. Mary YS et al (2014) Quantum mechanical and spectroscopic (FT-IR, FT-Raman, 1H NMR and UV) investigations of 2-(phenoxymethyl) benzimidazole. Spectrochim Acta Part A 125:12–24
38. Anto P et al (2007) Vibrational spectroscopic studies and ab initio calculations of 5-methyl-2-(p-fluorophenyl) benzoxazole. Spectrochim Acta A 67(3–4):744–749
39. Santagneli SH et al (2007) Structural Studies of $NaPO_3$–MoO_3 glasses by solid-state nuclear magnetic resonance and Raman spectroscopy. J Phys Chem B 111(34):10109–10117
40. Aboussatar M et al (2017) Phase equilibria in the NaF–CdO–$NaPO_3$ system at 873 K and crystal structure and physico-chemical characterizations of the new Na_2CdPO_4F fluorophosphate. J Solid State Chem 248:75–86
41. Forster Paul M et al (2005) A high-throughput investigation of the role of pH, temperature, concentration, and time on the synthesis of hybrid inorganic–organic materials. Angew Chem Int Ed 44:7608–7611

42. Sha J et al (2008) pH-dependent assembly of hybrids based on wells-dawson POM/Ag chemistry. Inorg Chem 47(12):5145–5153
43. Vijayan N et al (2004) Growth and characterization of benzimidazole single crystals: a nonlinear optical material. J Cryst Growth 262(1–4):490–498
44. ElBatal F et al (2011) UV–visible and infrared absorption spectra of gamma irradiated V_2O_5-doped in sodium phosphate, lead phosphate, zinc phosphate glasses: a comparative study. J Non-Cryst Solids 357(3):1027–1036
45. Vijayan N et al (2004) Growth and characterization of benzimidazole single crystals: a nonlinear optical material. J Cryst Growth 262(1–4):490–498
46. Chandra A (2010) Hot-pressed Na^+ ion conducting solid polymer electrolytes: (1−x) PEO: x $NaPO_3$. Eur Phys J Appl Phys 50(2):21103
47. Bhide A, Hariharan K (2006) A new polymer electrolyte system (PEO)n: $NaPO_3$. J Power Sources 159(2):1450–1457
48. Bhide A, Hariharan K (2007) Sodium ion transport in $NaPO_3$–Na_2SO_4 glasses. Eur Polym J 43:4253–4270
49. Driss Rair et al (2018) Spectroscopic and thermal degradation studies of novel hybrid polymer based on sodium polyphosphate–polystyrene. Mediter J Chem 7(5):337–345
50. Tang C, Yang Z (2017) Transmission electron microscopy (TEM) chapter 8. Membrane characterization. Elsevier, Amsterdam, pp 145–159